

# Disentangling Visual Transformers: Patch-level Interpretability for Image Classification

Guillaume Jeanneret<sup>\*,†</sup>, Loïc Simon<sup>†</sup>, Frédéric Jurie<sup>†</sup>

<sup>\*</sup>ISIR - Sorbonne University

<sup>†</sup>Normandy University, ENSICAEN, UNICAEN, CNRS, GREYC

## Abstract

*Visual transformers have achieved remarkable performance in image classification tasks, but this performance gain has come at the cost of interpretability. One of the main obstacles to the interpretation of transformers is the self-attention mechanism, which mixes visual information across the whole image in a complex way. In this paper, we propose Hindered Transformer (HiT), a novel interpretable by design architecture inspired by visual transformers. Our proposed architecture rethinks the design of transformers to better disentangle patch influences at the classification stage. Ultimately, HiT can be interpreted as a linear combination of patch-level information. We show that the advantages of our approach in terms of explicability come with a reasonable trade-off in performance, making it an attractive alternative for applications where interpretability is paramount.*

## 1. Introduction

Deep learning architectures have achieved remarkable breakthroughs in domains such text [19], vision [20, 46], or multimodal tasks [37], prompting widespread interest in their application to real-world problems [34]. However, as these models are increasingly used in high-stakes scenarios, understanding their decision-making process becomes crucial to ensure their decisions are grounded in meaningful variables rather than spurious correlations [4, 28]. This necessity has driven the development of trustworthy and interpretable architectures.

Interpretable-by-Design (ID) architectures [14] aim to inherently explain their decision-making process, eliminating the need for external interpretability tools. Ideally, these architectures maintain comparable performance to traditional black-box methods while providing insights into their internal workings. Despite their promise, existing ID architectures largely rely on convolutional neural networks

(CNNs) as feature extractors [7, 32, 45, 66]. Given the recent success of transformer-based models [18], transitioning to interpretable transformers is a logical next step.

Although Vision Transformers (ViTs) [18] have demonstrated superior performance in computer vision tasks, the literature on their explainability and interpretability remains sparse. While attention maps are sometimes considered interpretable, many studies [26, 55] argue that they provide little to no insight into the actual decision-making process. We concur that attention maps offer only partial and insufficient cues, and instead route towards ID architectures.

In this paper, we address this gap by introducing a novel interpretable transformer-like architecture. Our proposed model, the Hindered Transformer (HiT), advances the understanding of ViTs by analyzing the flow of individual image patches and decomposing the classification token (**CLS**) into contributions from each individual token. By constructing predictions as the sum of these token contributions, HiT achieves interpretability without relying on external methods [3] or gradient-based approaches [58], classifying it as an ID method.

We summarize our contributions as follows: i) We propose the Hindered Transformer (HiT) backbone, a variant of vision transformers that is inherently interpretable. ii) We empirically validate HiT on six datasets – ImageNet [16], CUB 2011 [65], Stanford Dogs [30], Stanford Cars [33], FGVC-Aircraft [40], and Oxford-IIIT Pets [48] – demonstrating its interpretability both quantitatively and qualitatively, outperforming recent ID transformer-based models and post-hoc methods.

Our code and pretrained models are found on [GitHub](#)

## 2. Related Work

The performance of neural networks on computer vision tasks is well-established, but the complexity of these models can make them difficult to understand. This lack of transparency is problematic and has motivated the scientific community to develop methods for making neural networks more interpretable. There are two main approaches

<sup>‡</sup> Work done at GREYC Laboratory, now at ISIR Laboratory

to this problem: post-hoc methods, which seek to analyze an already-trained model, and interpretable by design architectures, which aim to create models whose decision-making processes are inherently transparent.

Many post-hoc methods have been proposed in the literature, including counterfactual explanations [4, 29, 72], saliency maps [27, 50, 54, 68], and model distillation [22, 59]. Closer to our work, a few attempts have been made to explain a ViT architecture via post-hoc algorithms. For instance, Abnar and Zuidema [1] proposed to compute a score per token by recursively propagating the attention maps in a top-bottom approach. In addition, some methods extended the LRP [6] paradigm to include the attention heads [12, 13]. The previous methods leverage the mechanisms of transformers to estimate the individual contribution of each token. While these approaches provide insights into trained models, they often rely on external tools or post-processing, which can limit their generalizability and integration into the model itself.

The field of interpretable by design architectures is diverse, as there is no single approach to explaining the complex behaviors neural networks. While many methods have been proposed, there has been a recent focus on prototypical part networks, such as ProtoPNets introduced by Chen *et al.* [14]. ProtoPNets computes class predictions based on the distances between patches of the final feature map and some prototypes, which can be visualized. Additionally, there have been many variations of ProtoPNets proposed in the literature [8, 11, 15, 17, 23, 42–44, 53, 62, 66, 67]. These variations aim to refine ProtoPNets to enhance performance and interpretability but primarily focus on convolutional neural networks (CNNs) [24, 57], limiting their application to modern transformer architectures.

In addition to ProtoPNets, there are other methods that use alternative forms of prototypes. For example, PDiscoNet [63] automatically detects parts of objects and uses them for the final classification. Similarly, BagNet [9] mimics the Bag-of-Features approach to understand the decision-making process. Concept Bottleneck Models [32, 45] use concepts to explain their decisions. Finally, a family of networks propose interpretable layers, such as B-cos networks [7], that learns an easily interpretable input-dependent linear transformation. The work of Zhang *et al.* [73] proposed convolutional interpretable layers. Finally, some works use some variation of decoupled networks [35, 36, 56] to highlight what a filter is looking at.

Concerning visual transformers, several recent works have attempted to make transformers more interpretable by modifying their architecture. Some papers try to push the boundaries to include transformer-based heads [25, 31, 49, 52] for prototype interpretability. However, they only include a single self-attention mechanism on top of a CNN backbone. ProtoPFormer [69] suggests including a ViT

backbone in the prototype setup. To do this, ProtoPFormer includes a prototype layer on top of both the classification and image tokens. While innovative, this architecture does not ensure that the tokens contain purely local information due to the increased receptive fields of tokens when combining classification and image tokens [51]. B-cos networks V2 [10] use the same rationale as the original B-cos [7] approach, but they extend it to transformers. In a few words, B-cos networks summarize their inner workings as a single linear function, creating the attribution map by simply multiplying the input and the summarized network. However, this extension still relies on convolutional layers as the initial feature extraction stage, limiting its interpretability scope. Finally, A-ViT [70] was originally designed for faster inference by removing tokens at certain layers. Despite this, this mechanism serves as an interpretable system, as the most important tokens are retained until the last layer. This approach, however, focuses on efficiency rather than interpretability as its primary goal.

In contrast with this literature, we propose an architecture interpretable by design, by adapting the main building blocks of vision transformers to disentangle the contributions of each image patch. This enables us to compute the salient regions of the image without the need for any non-traditional training or invasive methods. Unlike other approaches, we avoid relying on the attention mechanism of the multi-head attention (MHA) block to produce saliency maps. Instead, our network inherently generates these maps as part of its decision-making process.

### 3. Methodology

In this section, we present our proposed approach and the rationale behind it. First, in §3.1, we present the preliminaries for the multi-head attention mechanism and ViTs. Next, in §3.2 we will show that attention and multi-head attention output can be decomposed into the individual contributions of the inputs. Finally, in §3.3 we present our novel architecture, the Hindered Transformer (HiT). The core of our method is to minimise the mixing of patch-level information, which allows us to express the classification token (**CLS**) in ViTs as the sum of individual tokens, a direct result of §3.2. In other words, this simplification allows us to check the contribution of each token.

#### 3.1. Preliminaries: Transformers, ViTs and Notations

The transformer architecture is built upon the Scaled Dot-Product Attention operation [64], commonly referred to as *attention*. Given a query token sequence  $x^q \in \mathbb{R}^{L_q \times d_{model}}$  and a target sequence (or key-value sequence)  $x^t \in \mathbb{R}^{L_t \times d_{model}}$ , where  $L_q$  and  $L_t$  are their respective sequence lengths and  $d_{model}$  is the token dimension, the attention

mechanism is computed as follows:

$$\begin{aligned} Q &= x^q W_Q + b_Q \\ K &= x^t W_K + b_K \\ V &= x^t W_V + b_V \\ A(x^q, x^t) &= \text{softmax} \left( \frac{QK^T}{\sqrt{d_k}} \right) V \end{aligned} \quad (1)$$

where the output is a sequence of the same length as  $x^q$ ,  $d_k$  is the dimension of the linear transformations, and  $W_i \in \mathbb{R}^{d_{model} \times d_k}$  and  $b_i \in \mathbb{R}^{d_k}$  are the weights of the linear projection  $i \in \{Q, K, V\}$ . In addition, Vaswani *et al.* [64] proposed to compute the attention mechanism  $h$  times in parallel, setting  $d_k = d_{model}/h$  for each individual attention operation. The resulting vectors of each individual attention, formally called heads, are concatenated and linearly post-processed to obtain the final result. This operation is called multi-head attention, and it is described as follows:

$$MHA(x^q, x^t) = \underbrace{[A^1(x^q, x^t); \dots; A^h(x^q, x^t)]}_{\text{Concatenate } h \text{ times}} W_o + b_o, \quad (2)$$

with  $A^i$  being the  $i^{th}$  attention mechanism in the MHA, and  $W_o \in \mathbb{R}^{d_{model} \times d_{model}}$  and  $b_o \in \mathbb{R}^{d_{model}}$  the linear transformation parameters.

In computer vision, to incorporate image data into this sequence-based formulation, the ViT first partitions the input image into  $N^2$  equal-sized patches and linearly projects them to create the patch token sequence. Additionally, following standard practice, a learnable classification token **CLS** is prepended to the patch sequence. Finally, each patch token is summed with a positional embedding to encode its spatial location within the image. For the remainder of the paper, the sequence  $x \in \mathbb{R}^{(N^2+1) \times d_{model}}$  denotes the concatenation of the patch tokens and the **CLS** token, where  $x[0]$  corresponds to the **CLS** token.

The main ViT block builds on the MHA operation, followed by a token-wise MLP block, as in text-based transformers. Formally, given a set of patches  $x_l$  at layer  $l$ , the ViT block first computes a globalized set of tokens using the MHA block. The resulting output is summed with a skip connection. Then, the output is fed into a token-wise MLP to post-process each token, followed, again, by a skip connection. This block is summarized as follows

$$\begin{aligned} x'_l &= x_l + MHA(x_l, x_l) \\ x_{l+1} &= x'_l + MLP(x'_l) \end{aligned} \quad (3)$$

Note that before the MHA and MLP blocks, a LayerNorm [5] operation is applied to the data sequence, but for simplicity, we omit this operation. Finally, the **CLS** token is fed into a LayerNorm followed by a linear classifier to produce the logits of the classification task.

For the rest of the paper, we will use the terms token and patch interchangeably, referring to the image patch tokens.

### 3.2. Multi-Head Attention and Patch Mixing in Transformers

In this section, we aim to decompose the MHA operation to demonstrate that it is possible to retrieve the individual contributions of each token. In this way, we aim to lay the foundation for our architecture, which is described in the next section.

Let's start by focusing on the attention operation (Eq. 1). Since we will focus on the **CLS** token later, and to simplify the analysis, let's assume that the query sequence has length  $L_q = 1$ . Consequently, the attention mechanism can be rewritten as

$$A(x^q, x^t) = \sum_{v \in x^t} s(v, x^q, x^t) (v W_V + b_v), \quad (4)$$

where  $s(v, x^q, x^t) \in \mathbb{R}$  is the contribution factor of  $v \in x^t$ , computed via the softmax operation in Eq. 1. Here, Eq. 4 shows that we can decompose the attention mechanism into separately processed patches - each patch  $v$  in  $x^t$  adds  $s(v, x^q, x^t) (v W_V + b_v)$ . Accordingly, if  $x^t$  contains purely local information, the output of the attention is a *weighted sum of local data*. Here, we define whether a token contains local information as the product of processing a single patch without the influence of other datapoints.

To continue, we incorporate the previous observation into multi-head attention and verify that we can still unroll this operation into a *sum of separate vectors*. One might be concerned that the concatenation-linear operation will mix each token. However, we argue that the result is still valid, since concatenating and linearly transforming the resulting vector is equivalent to linearly transforming each head and adding them together. Formally, by denoting  $W_v^i$  and  $b_v^i$  as the weights of the linear transformation generating the value sequence of  $i^{th}$  head, and breaking apart  $W_o$  into  $h$  separate matrices,  $W_o = [W_o^1; W_o^2; \dots; W_o^h]$ , with  $W_o^i \in \mathbb{R}^{d_k \times d_{model}}$ , then, the MHA becomes

$$\begin{aligned} MHA(x^q, x^t) &= b_o + \sum_{v \in x^t} v'(v) \\ \text{where } v'(v) &= \sum_{i=1}^h s(v, x^q, x^t) (v W_v^i + b_v^i) W_o^i. \end{aligned} \quad (5)$$

The previous result implies that we can still decompose the MHA result as the sum of vector patches, regardless of the number of heads in the MHA. So the same conclusion holds as in Eq. 4: if the content in  $x^t$  is local, then we can unravel the MHA mechanisms into *local contributions*.

### 3.3. Untangling Visual Transformers

Unlike single MHA layers, ViTs operate on global features. To integrate local information, these architectures use two

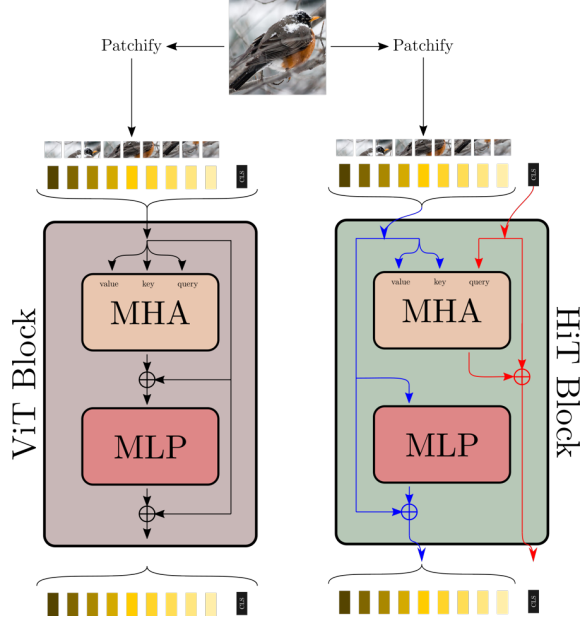


Figure 1. **ViT and HiT blocks.** While the ViT block mixes the patch data, HiT uniquely updates the **CLS** via the MHA, but avoids post-processing the classification token in the MLP, allowing the **CLS** to be unrolled at the last layer as individual contributions.

mechanisms: the MHA layers, which spread the information within tokens, and the nonlinear MLPs, which introduce complex correlations even when applied to a linear combination of local contributions. For better explainability, it would be ideal if the classifier’s decision could be expressed as a combination of information from individual patches, allowing a more interpretable understanding of how local information contributes to global predictions.

In this section, we describe our proposed architecture: Hindered Transformer (HiT). By constraining the image tokens to contain only local information along all inference blocks, and by avoiding mixing the **CLS** token, our novel method is able to partition the **CLS** token into each individual patch, a direct outcome of the previous section. Fig. 1 shows the difference between the ViT block, and our block.

The first challenge is then constraining the data flow between patches. To do so, we create an intermediate architecture that uses **CLS** token  $x_l[0]$  as the query in the MHA operation, and the rest of the sequence  $x_l$  as the key-value input. So, the output from the MHA is a single token that is summed to  $x_l[0]$ . Then, as in ViTs, we will post-process each token in the sequence with the MLP. Thus, the ViT update function in Eq. 3 is transformed to

$$\begin{aligned} x'_l[0] &= x_l[0] + MHA(x_l[0], x_l[1:]) \\ x'_l[1:] &= x_l[1:] \\ x_{l+1} &= x'_l + MLP(x'_l). \end{aligned} \quad (6)$$

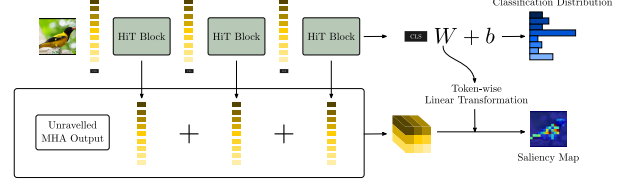


Figure 2. **Saliency Maps computation using HiT.** From the results from §3.2 and the definition of our architecture, HiT enables to extract the individual contribution per token and per layer. By adding together all tokens per layer, we can rearrange the tokens in a spatial layout and use the linear layer *à la* CAM [74] to extract the contribution of each token.

The previous model solves one problem by limiting the merging of data in local patches. However, processing the **CLS** token through the MLP mixes the local information provided by the MHA block, as well as the value and output operations. Since our goal is to disentangle the data flow into individual contributions, we need to further constrain this processing. To do this, we simply avoid updating the **CLS** token through the MLP and passing it to the target sequence. So, our block inference is

$$\begin{aligned} x_{l+1}[0] &= x_l[0] + MHA(x_l[0], x_l[1:]) \\ x_{l+1}[1:] &= x_l[1:] + MLP(x_l[1:]) \end{aligned} \quad (7)$$

We call the final architecture the Hindered Transformer (HiT), as we hinder the connections of the ViT. In a nutshell, HiT only updates the **CLS** token via the MHA, while the MLP blocks update the image patches. These restrictions help to preserve purely local information in each token, while allowing the **CLS** token to be unrolled.

Since the classification token is not post-processed with MLP or MHA, the final image classification is the sum of the individual tokens in all layers, as shown in §3.2. Therefore, the **CLS** in the last layer is

$$\begin{aligned} x_L[0] &= x_0[0] + \sum_{l=0}^{L-1} MHA(x_l[0], x_l[1:]) \\ &= x_0[0] + \sum_{l=0}^{L-1} \left[ b_o^l + \sum_{v \in x_l[1:]} v'_l(v) \right] \\ &= \sum_{l=0}^{L-1} \sum_{v \in x_l[1:]} \left[ v'_l(v) + \frac{b_o^l}{N^2} + \frac{x_0[0]}{LN^2} \right]. \end{aligned} \quad (8)$$

Please note that we distribute the biases  $b_o^l$  of the projection operation in the MHA head evenly to each patch  $v'_l(v)$ . In a similar fashion, we spread  $x_0[0]$  into all tokens for all layers.

One advantage of this architecture is that we can easily compute saliency maps, as shown in Fig. 2. The double sum in Eq. 8 can be decomposed as a tensor  $\mathbb{R}^{L \times N^2 \times d_{model}}$ ,



where the final image representation is the sum over the first and second dimensions, *i.e.* the layer and token dimension, respectively. Thus, and similarly to CAM [74], to compute the regions of interest used by the model for an input image, we simply run the linear classifier on each patch to get the map. This rationale is similar to the LRP [6] method in the sense that the sum of value in the saliency is equal to the output logit for that specific class.

### 3.4. Token Pooling

Token pooling [41], which involves downsampling the number of tokens as one progresses through the layers, is commonly used to improve the computational efficiency of standard transformers [47]. This pooling technique effectively addresses the issue of representation power (as empirically demonstrated in § 4.7) by expanding the receptive field of the image tokens in the deeper layers. We choose to adopt this approach due to its significant advantages.

To achieve this, we first reorganize the tokens into their spatial layout and then perform the pooling operation. However, we need to adapt the explanation generation approach to accommodate the pooled tokens. Typically, this involves using the backward operation of the pooling operator. In our case, since we rely on average pooling, which is linear, the backward operation is simply the transposed operator, which replicates each output token across the associated  $2 \times 2$  block and divides by 4. In other words, we distribute the importance of the pooling step equally among the contributing tokens.

## 4. Experiments

### 4.1. Evaluation Protocols

The quantitative evaluation of the saliency map quality is performed using the insertion-deletion metrics [50]. The insertion process is performed iteratively by creating a perturbed copy of the input image by progressively adding regions from the original image. This copy is initially filled either with zeros or with a blurred version of the image. Starting with the most influential regions according to the saliency map and moving to the least influential regions, each step adds an original region in place of the perturbed one. During this process, the class probability of the perturbed image is tracked for the originally predicted class. This results in a curve for each input image, where the x-axis represents the percentage of inserted regions and the y-axis represents the probability. Then, the insertion metric is computed with the area under the curve (AUC) of the mean probability curve for all tested instances. The deletion metric works in a similar fashion, removing the original patches starting with the most influential and continuing until all patches are removed. If a saliency map generator accurately identifies the most relevant components influenc-

ing the model’s decision, it will produce a steep increase (or decrease) in the insertion (or deletion) curve. A sharp transition in these curves confirms that the highlighted regions are indeed those utilized by the model for classification. Consequently, a reliable saliency method will achieve a higher (lower) AUC for the insertion (deletion) metric.

Insertion-deletion curves generated by different models cannot be directly compared if the models do not have the same calibration of their outputs, which is the case in these experiments. Therefore, we propose normalizing the insertion-deletion metrics by calculating the normalized AUC (nAUC). This normalization adjusts the mean probability curve based on the maximum and minimum values of the curve before computing the AUC.

Lastly, when assessing interpretable by-design approaches, it is necessary to evaluate the trade-off between raw performance on the task vs the gain in interpretability. Specifically, we compare the top-1 accuracy in contrast to the insertion-deletion metrics.

As for the dataset, we evaluated HiT on six diverse image classification datasets, traditionally used for evaluating interpretability architectures: ImageNet [16], CUB-2011 [65], Stanford Dogs [30], Stanford Cars [33], FGVC-Aircraft [40], and Oxford-IIIT Pets [48]. In the supplementary material, we described in-depth each dataset.

### 4.2. Implementation Details

To train HiT on ImageNet [16], we used the official DeiT3 codebase [61] and followed a similar setup to their method. Please read the supplementary for more details on the architecture, but in short, HiT uses exactly the same depth and number of layers as ViT. For HiT-B and HiT-S, we trained our models for 600 epochs using the AdamW optimizer [39] with a learning rate of  $8 \times 10^{-4}$ , a weight decay of 0.05, a batch size of 4096, 20 warm-up epochs, a cosine annealing scheduler [38], and ThreeAugment [61] data augmentation. Unlike the DeiT3 training regime, we did not use the binary cross entropy loss or any LayerDrop [21] regularization, but the traditional cross entropy with a smoothing of 0.1 and an attention dropout of 0.2. To fine-tune HiT in the other datasets, we trained our models similarly to the ImageNet’s configuration, but instead we set the batch size to 512, the number of epochs to 300 and the learning rate to  $5 \times 10^{-5}$  for Stanford Dogs and Oxford Pets,  $4 \times 10^{-4}$  for Stanford Cars and FGVC-Aircraft, and  $1 \times 10^{-4}$  for CUB 2011.

### 4.3. Quantitative Evaluation of HiT

In Fig. 1, we compare the normalized insertion-deletion curves obtained from HiT and other baseline models using the blur strategy, as established in the literature. The baselines assessed include A-ViT [70], B-cos [10], and DeiT-B [60]. For B-cos, the saliency maps are intrinsically generated, while for DeiT-B, we rely on post-hoc extraction

Method	ImageNet		CUB 2011		Stanford Cars		Stanford Dogs		FGVC-Aircrafts		Oxford-IIIT Pets	
	I-Z ( $\uparrow$ )	D-Z ( $\downarrow$ )	I-Z ( $\uparrow$ )	D-Z ( $\downarrow$ )	I-Z ( $\uparrow$ )	D-Z ( $\downarrow$ )	I-Z ( $\uparrow$ )	D-Z ( $\downarrow$ )	I-Z ( $\uparrow$ )	D-Z ( $\downarrow$ )	I-Z ( $\uparrow$ )	D-Z ( $\downarrow$ )
HiT	<b>0.57</b>	<b>0.12</b>	<b>0.36</b>	<b>0.06</b>	<b>0.66</b>	<b>0.09</b>	<b>0.64</b>	<b>0.13</b>	<b>0.60</b>	<b>0.08</b>	<b>0.67</b>	<b>0.18</b>
HiT + Rollout	0.40	0.21	0.47	0.19	0.49	0.16	0.50	0.21	0.52	0.11	0.58	0.29
HiT + GradCAM	0.49	0.15	0.33	0.10	0.57	0.13	0.60	0.15	0.53	0.09	0.64	0.25
	I-B ( $\uparrow$ )	D-B ( $\downarrow$ )	I-B ( $\uparrow$ )	D-B ( $\downarrow$ )	I-B ( $\uparrow$ )	D-B ( $\downarrow$ )	I-B ( $\uparrow$ )	D-B ( $\downarrow$ )	I-B ( $\uparrow$ )	D-B ( $\downarrow$ )	I-B ( $\uparrow$ )	D-B ( $\downarrow$ )
HiT	<b>0.58</b>	<b>0.23</b>	<b>0.52</b>	<b>0.14</b>	<b>0.61</b>	<b>0.20</b>	<b>0.62</b>	<b>0.27</b>	<b>0.59</b>	<b>0.17</b>	<b>0.60</b>	<b>0.26</b>
HiT + Rollout	0.45	0.31	0.47	0.19	0.52	0.28	0.53	0.35	0.55	0.2	0.53	0.35
HiT + GradCAM	0.53	0.28	0.49	0.21	0.56	0.26	0.61	0.31	0.57	0.19	0.60	0.32

Table 1. **HiT and Explainability methods:** We quantitatively compare HiT maps and those created by GradCAM and the modified rollout matrix (mean attention) using AUC (no normalization required here). The assessment shows that HiT maps are more faithful than those generated by GradCAM or the rollout matrix. Higher insertion is better, while lower deletion is better. I and D refers to the Insertion and Deletion metrics, respectively. Z is the zero-corrupted image, while B is the blurred corruption strategy.

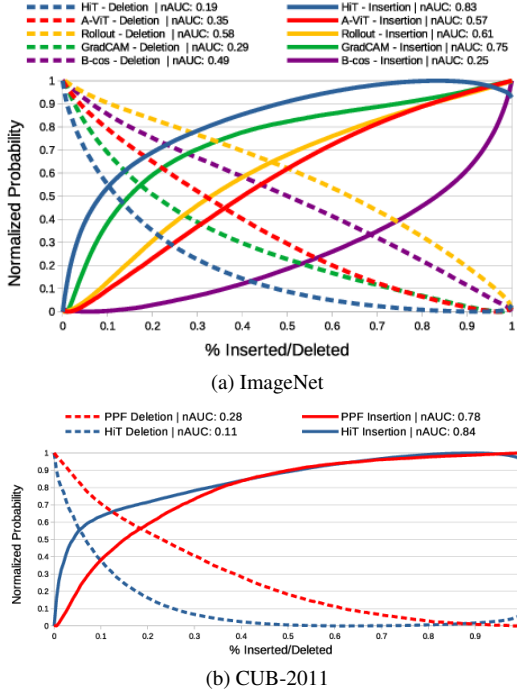


Figure 3. **Interpretability comparison.** We tested whether HiT’s saliency maps provide better information than ProtoFormer’s, A-ViT’s maps, B-cos, the rollout attention, and GradCAM. The results indicate that our methods are indeed more interpretable.

methods. Specifically, we use the Rollout Matrix [1] and GradCAM [54], referred to as DeiT-R and DeiT-GC, respectively. To create A-ViT saliency map, we utilized the layer where tokens were discarded, as described in their paper. Additionally, to mitigate the bias of the sorting algorithm when selecting the most important tokens (which tends to favor top-left corner tokens first), we added a small amount of random noise to the saliency map.

Additionally, we evaluate ProtoFormer [69] on the CUB-2011 dataset. ProtoFormer employs a Rollout Matrix to filter out irrelevant tokens for its final computation, and we used this Rollout Matrix to define the salient regions

Model	Interp.	IMNet	CUB	Dogs	Cars	Aircraft	Pets
DeiT3-B	X	83.6	84.9	94.0	92.8	85.3	95.0
DeiT-B	X	81.1	84.9	93.4	93.0	84.9	95.1
B-cos-B	✓	74.4	-	-	-	-	-
HiT-B	✓	75.0	79.0	86.8	86.2	79.8	88.6
DeiT3-S	X	81.4	83.1	90.6	93.0	83.9	94.5
DeiT-S	X	79.8	83.0	89.6	92.4	83.4	94.3
A-ViT-S	✓	78.6	-	-	-	-	-
B-cos-S	✓	69.2	-	-	-	-	-
ProtoFormer-S	✓	-	84.9	90.0	90.9	-	-
HiT-S	✓	71.4	76.1	80.3	85.2	77.4	88.5

Table 2. **Top1 Accuracy.** Our proposed models have a clear performance loss compared to other ViTs. However, the ViT gains come at the expense of interpretability, whereas the HiT has acceptable performance while being explicable. ProtoFormer performance were extracted from their paper.

for the insertion-deletion analysis.

The results of this experiment are presented in Fig. 3a for ImageNet and Fig. 3b for CUB-2011. The nAUC scores and the profiles of the curves indicate that HiT outperforms other ID methods in terms of interpretability.

To further enhance our understanding of HiT’s interpretability, we analyze the unnormalized insertion-deletion metrics of traditional post-hoc methods compared to HiT in Tab. 1. Specifically, we compare the saliency maps extracted from HiT with those generated by GradCAM [54] and an adapted Rollout Matrix [1], both computed on HiT. Overall, the inherent saliency maps of HiT demonstrate superior performance compared to the post-hoc methods for both insertion and deletion metrics. This finding suggests that these post-hoc algorithms do not consistently identify the regions used for classification.

Finally, in Tab. 2, we present the accuracy performance of our proposed architecture compared to both non-interpretable and interpretable alternatives. As expected, all interpretable architectures, with the exception of ProtoFormer, show a decrease in performance relative to the non-interpretable baseline. However, our Hindered Transformer maintains clear advantages in interpretability without a significant drop in performance.

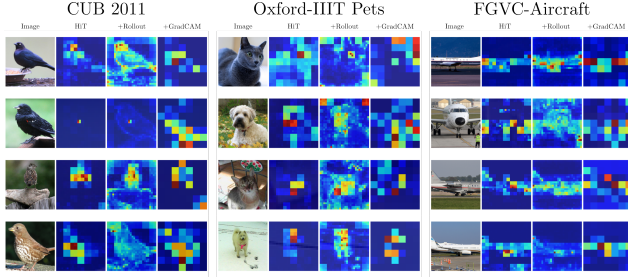


Figure 4. **Qualitative Comparison.** We show the image and its saliency maps produced by HiT and their homologous using Rollout and GradCAM. We noticed that HiT tends to use the object’s features in the image for its prediction, independently if its prediction is erroneous or not.

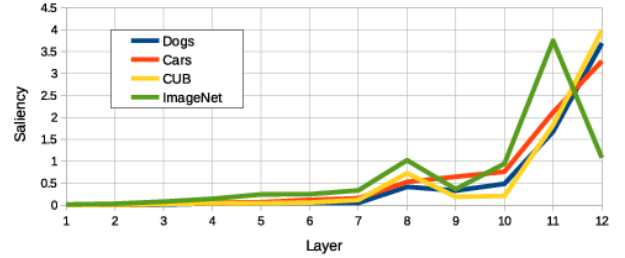
#### 4.4. Qualitative Evaluation

In the next part of our study, we show in Fig. 4 a qualitative comparison between the saliency maps generated by HiT and those computed with GradCAM and the Rollout Matrix when applied to HiT. We make three main conclusions. First, we found that our method focuses on certain parts of objects, regardless of whether the prediction is accurate or not. To quantify our claim, we computed the center of mass for each explanation and checked whether it fell within the object’s bounding box in the CUB test set. We achieved 93.4% accuracy, which strongly supports our claim. Second, our qualitative analysis suggests that misclassification generally occurs due to similar features between image classes. However, since our method generates saliency maps, HiT inherently adopts their weaknesses: it shows where the decision was made, but not which features were used. Third, Rollout and GradCAM produce noisy maps. For example, the former shows edges and highlights the general shape of the object, while the latter produces misaligned coarse maps with our base model.

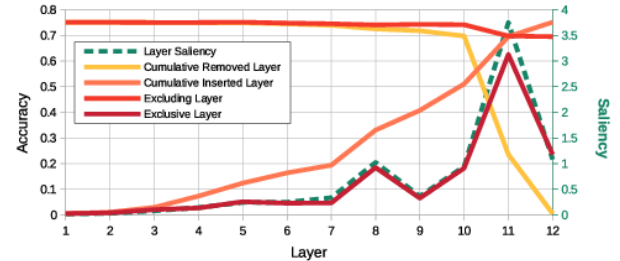
#### 4.5. Layer-wise Contribution

Another advantage of HiT is that we can compute the contribution of each layer. Similar to computing the saliency maps spatially, we can create the layer-wise output tokens and look for their individual contributions. To this end, we show the results in Fig. 5a for four tested dataset. Without any surprise, we can see that most of the discriminative features are in the final layers.

To ensure that our results are valid, we tested several ablations of our trained model on the ImageNet dataset, shown in Fig. 5b. For instance, we tested the accuracy drop by removing or adding a layer of choice (*Excluding/Exclusive Layer* in the figure). Similarly, we check the performance loss by removing/adding layers in a cascaded manner, dubbed *cumulative removed/inserted layer*. The results corroborate our previous conclusions: our novel architecture is capable of showing the contribution of each indi-



(a) Layer saliencies per dataset.



(b) Empirical validation of layer-wise saliency.

Figure 5. **Layer Saliency.** HiT has more advantages than just image saliency. (a) The first experiment shows that HiT computes the contribution per layer. Without any surprise, the final layers have a greater contribution. (b) We empirically validate our findings in ImageNet with a variety of experiments. Indeed, the results show that by removing certain layers, we obtain larger expected results congruent with the layer saliency.

vidual layer without relying on external methods, such as Linear Probing [3], to understand the basic functioning of their inner layers.

#### 4.6. Sanity Check

Adebayo *et al.* [2] highlight that certain maps, such as edge detectors, may appear visually coherent, although they are actually unrelated to the model’s decision. In order to address this issue, they proposed sanity check, which involves the iterative randomisation of the parameters of the network layers. This process begins with the deepest layers and proceeds step-by-step to the shallower ones. The resulting saliency map produced at each randomization step is then compared with the original map. In our study, we adopt the same methodology as Adebayo *et al.* [2] and compute the absolute rank correlation between the original saliency map and the one generated after randomization, as shown in Fig. 6a. Additionally, we include the absolute Pearson correlation coefficient in Fig. 6b, and some examples in Fig. 6c.

Foremost, we noticed that the rank correlation has a steeper slope than the Pearson correlation for the linear classification layer. This shows that there is a greater similarity with the Pearson correlation. However, the values are relatively low (less than 0.5), indicating large variations. Secondly, both metrics reach a plateau for the subsequent randomized models. This low similarity suggests that the

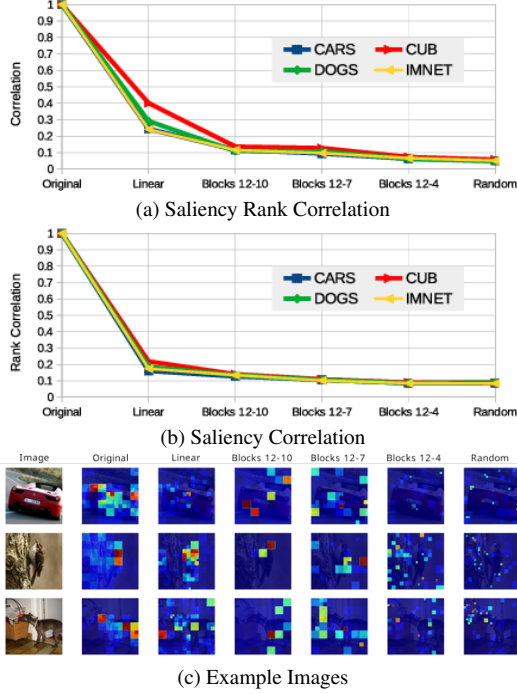


Figure 6. **Sanity checks on HiT.** We measure the (a) rank correlation and (b) Pearson correlation of HiT saliency maps before and after randomising the parameters of a layer. (c) Some visual examples of the saliency maps of randomised models.

salient regions highlighted by our model are indeed what the model sees. Finally, Fig. 6c shows some qualitative examples produced by the randomization of all blocks, showing that, effectively, the weights’ randomization reflect a large variation in the produced saliency.

#### 4.7. Ablating HiT

In §3.4, we suggested that token pooling layers will increase the representation power of HiT. We hypothesize that the lack of inter-token connections would downgrade greatly the performance. Thus, in this section, we empirically validate that the inclusion of token pooling layers increases the performance of the model. In addition, we implemented a more powerful pooling strategy used by IdentityFormer [71]: a 3×3 convolution with a stride of 2. We focus on this architecture because it shares similar characteristics with HiT, where each token contains its own information. Lastly, we theorize that optimizing HiT architectures is challenging. To address this, we adopt an approach similar to DeiT3 [61], training our model for 300 and 600 epochs. Finally, we observed that using binary cross-entropy adversely affects the model’s performance, contrary to its effect on DeiT3.

We present the results in Table 3. The findings align with our suspicions: the lack of transferred information between patches significantly reduces the model’s accuracy.

Architecture	Pooling	Loss	Epochs	Val ImageNet
HiT-S	None	XE	300	65.6
HiT-S	None	XE	600	67.8
HiT-S	2x2 AvgPool	XE	300	69.3
HiT-S	2x2 AvgPool	XE	600	<b>71.4</b>
HiT-S	None	BCE	400	59.9
HiT-S	None	BCE	800	62.6
HiT-B	None	XE	600	71.5
HiT-B	2x2 AvgPool	XE	600	<b>75.0</b>
HiT-s18	2x2 AvgPool	XE	300	65.6
HiT-s18	2x2 AvgPool	XE	600	69.3
HiT-s18	3x3 Conv	XE	300	<b>75.9</b>

Table 3. **Performance loss ablation.** HiT’s performance loss stems from the limited information shared between tokens. Concurrently, the results suggest that HiT’s optimization problem is more challenging, as extended training periods lead to more significant performance improvements.

For instance, by merely adding the convolutional pooling layer of IdentityFormer, we increase the accuracy of a HiT-s18 [71] from 65% to 75%. However, these convolutional layers compromise our model’s interpretability by entangling information between tokens. Despite this gain in performance, when HiT does not use pooling layers, its interpretability increases significantly, generating more precise explanations – please refer to the supplemental material for an empirical comparison. In addition, the binary cross entropy reduces its performance. Finally, unlike DeiT3 training schemes, our network benefits significantly from increasing the number of epochs. We believe that this result indicates HiT has not yet converged.

## 5. Conclusions

This paper proposed a novel interpretable transformer-like architecture: Hindered Transformer. HiT enhances interpretability by decoupling contributions from individual image patches, enabling the extraction of saliency maps without external tools. Extensive experiments across multiple datasets demonstrated the improved interpretability benefits from HiT with a reasonable drop in performance. HiT presents a promising approach, offering favorable trade-offs for applications where interpretability is critical.

Even though our proposed architecture has many advantages in the terms of interpretability, HiT has limiting factors: slow convergence and the potential challenges in capturing complex dependencies. Regarding the former, we believe that a more comprehensive hyperparameter search, which we were unable to conduct due to limited computational resources, could significantly reduce the training time. Regarding the latter, HiT has some token interactions during the self-attention mechanism, yet, it is indeed weaker than standard ViTs. This is troublesome for spatial tasks and would require substantial modifications, opening opportunities for future research.

**Acknowledgements** This work was supported by the Agence Nationale pour la Recherche (ANR) under award number ANR-19-CHIA-0017.



## References

- [1] Samira Abnar and Willem Zuidema. Quantifying attention flow in transformers. In *Annual Meeting of the Association for Computational Linguistics*, 2020. 2, 6, 12, 13
- [2] Julius Adebayo, Justin Gilmer, Michael Muelly, Ian Goodfellow, Moritz Hardt, and Been Kim. Sanity checks for saliency maps. In *Advances in Neural Information Processing Systems*. Curran Associates, Inc., 2018. 7
- [3] Guillaume Alain and Yoshua Bengio. Understanding intermediate layers using linear classifier probes. In *5th International Conference on Learning Representations, ICLR 2017, Toulon, France, April 24-26, 2017, Workshop Track Proceedings*. OpenReview.net, 2017. 1, 7
- [4] Maximilian Augustin, Valentyn Boreiko, Francesco Croce, and Matthias Hein. Diffusion visual counterfactual explanations. In *Advances in Neural Information Processing Systems*, 2022. 1, 2
- [5] Lei Jimmy Ba, Jamie Ryan Kiros, and Geoffrey E. Hinton. Layer normalization. *CoRR*, abs/1607.06450, 2016. 3
- [6] Sebastian Bach, Alexander Binder, Grégoire Montavon, Frederick Klauschen, Klaus-Robert Müller, and Wojciech Samek. On pixel-wise explanations for non-linear classifier decisions by layer-wise relevance propagation. *PloS one*, 10 (7):e0130140, 2015. 2, 5
- [7] Moritz Böhle, Mario Fritz, and Bernt Schiele. B-cos networks: Alignment is all we need for interpretability. In *IEEE/CVF Conference on Computer Vision and Pattern Recognition, CVPR 2022, New Orleans, LA, USA, June 18-24, 2022*, pages 10319–10328. IEEE, 2022. 1, 2
- [8] Andrea Bontempelli, Stefano Teso, Katya Tentori, Fausto Giunchiglia, and Andrea Passerini. Concept-level debugging of part-prototype networks. In *The Eleventh International Conference on Learning Representations*, 2023. 2
- [9] Wieland Brendel and Matthias Bethge. Approximating CNNs with bag-of-local-features models works surprisingly well on imagenet. In *International Conference on Learning Representations*, 2019. 2
- [10] Moritz Böhle, Navdeep Singh, Mario Fritz, and Bernt Schiele. B-cos alignment for inherently interpretable cnns and vision transformers. *IEEE Transactions on Pattern Analysis and Machine Intelligence*, pages 1–15, 2024. 2, 5
- [11] Zachariah Carmichael, Suhas Lohit, Anoop Cherian, Michael J Jones, and Walter J Scheirer. Pixel-grounded prototypical part networks. In *Proceedings of the IEEE/CVF Winter Conference on Applications of Computer Vision*, pages 4768–4779, 2024. 2
- [12] Hila Chefer, Shir Gur, and Lior Wolf. Transformer interpretability beyond attention visualization. In *Proceedings of the IEEE/CVF Conference on Computer Vision and Pattern Recognition (CVPR)*, pages 782–791, 2021. 2
- [13] Hila Chefer, Shir Gur, and Lior Wolf. Generic attention-model explainability for interpreting bi-modal and encoder-decoder transformers. In *Proceedings of the IEEE/CVF International Conference on Computer Vision*, pages 397–406, 2021. 2
- [14] Chaofan Chen, Oscar Li, Daniel Tao, Alina Barnett, Cynthia Rudin, and Jonathan K Su. This looks like that: Deep learning for interpretable image recognition. In *Advances in Neural Information Processing Systems*. Curran Associates, Inc., 2019. 1, 2
- [15] Jifeng Dai, Haozhi Qi, Yuwen Xiong, Yi Li, Guodong Zhang, Han Hu, and Yichen Wei. Deformable convolutional networks. In *Proceedings of the IEEE International Conference on Computer Vision (ICCV)*, 2017. 2
- [16] Jia Deng, Wei Dong, Richard Socher, Li-Jia Li, Kai Li, and Li Fei-Fei. Imagenet: A large-scale hierarchical image database. In *2009 IEEE Conference on Computer Vision and Pattern Recognition*, pages 248–255, 2009. 1, 5, 12, 13
- [17] Jon Donnelly, Alina Jade Barnett, and Chaofan Chen. Deformable protopnet: An interpretable image classifier using deformable prototypes. In *Proceedings of the IEEE/CVF Conference on Computer Vision and Pattern Recognition*, pages 10265–10275, 2022. 2
- [18] Alexey Dosovitskiy, Lucas Beyer, Alexander Kolesnikov, Dirk Weissenborn, Xiaohua Zhai, Thomas Unterthiner, Mostafa Dehghani, Matthias Minderer, Georg Heigold, Sylvain Gelly, Jakob Uszkoreit, and Neil Houlsby. An image is worth 16x16 words: Transformers for image recognition at scale. In *International Conference on Learning Representations*, 2021. 1
- [19] Abhimanyu Dubey, Abhinav Jauhri, Abhinav Pandey, Abhishek Kadian, Ahmad Al-Dahle, Aiesha Letman, Akhil Mathur, Alan Schelten, Amy Yang, Angela Fan, Anirudh Goyal, Anthony S. Hartshorn, and *et al.* The llama 3 herd of models. *ArXiv*, abs/2407.21783, 2024. 1
- [20] Patrick Esser, Sumith Kulal, Andreas Blattmann, Rahim Entezari, Jonas Müller, Harry Saini, Yam Levi, Dominik Lorenz, Axel Sauer, Frederic Boesel, et al. Scaling rectified flow transformers for high-resolution image synthesis. In *Forty-first international conference on machine learning*, 2024. 1
- [21] Angela Fan, Edouard Grave, and Armand Joulin. Reducing transformer depth on demand with structured dropout. In *International Conference on Learning Representations*, 2020. 5
- [22] Yunhao Ge, Yao Xiao, Zhi Xu, Meng Zheng, Srikrishna Karanam, Terrence Chen, Laurent Itti, and Ziyan Wu. A peek into the reasoning of neural networks: Interpreting with structural visual concepts. In *Proceedings of the IEEE/CVF Conference on Computer Vision and Pattern Recognition (CVPR)*, pages 2195–2204, 2021. 2
- [23] Peter Hase, Chaofan Chen, Oscar Li, and Cynthia Rudin. Interpretable image recognition with hierarchical prototypes. In *Proceedings of the AAAI Conference on Human Computation and Crowdsourcing*, pages 32–40, 2019. 2
- [24] Kaiming He, Xiangyu Zhang, Shaoqing Ren, and Jian Sun. Deep residual learning for image recognition. In *2016 IEEE Conference on Computer Vision and Pattern Recognition (CVPR)*, pages 770–778, 2016. 2
- [25] Jinyung Hong, Keun Hee Park, and Theodore P Pavlic. Concept-centric transformers: Enhancing model interpretability through object-centric concept learning within a shared global workspace. In *Proceedings of the IEEE/CVF Winter Conference on Applications of Computer Vision*, pages 4880–4891, 2024. 2

- [26] Sarthak Jain and Byron C. Wallace. Attention is not explanation. In *North American Chapter of the Association for Computational Linguistics*, 2019. 1
- [27] Mohammad A. A. K. Jalwana, Naveed Akhtar, Mohammed Bennamoun, and Ajmal Mian. Cameras: Enhanced resolution and sanity preserving class activation mapping for image saliency. In *Proceedings of the IEEE/CVF Conference on Computer Vision and Pattern Recognition (CVPR)*, pages 16327–16336, 2021. 2
- [28] Guillaume Jeanneret, Loïc Simon, and Frédéric Jurie. Diffusion models for counterfactual explanations. In *Proceedings of the Asian Conference on Computer Vision (ACCV)*, 2022. 1
- [29] Guillaume Jeanneret, Loïc Simon, and Frédéric Jurie. Adversarial counterfactual visual explanations. In *Proceedings of the IEEE/CVF Conference on Computer Vision and Pattern Recognition (CVPR)*, 2023. 2
- [30] Aditya Khosla, Nityananda Jayadevaprakash, Bangpeng Yao, and Li Fei-Fei. Novel dataset for fine-grained image categorization. In *First Workshop on Fine-Grained Visual Categorization, IEEE Conference on Computer Vision and Pattern Recognition*, Colorado Springs, CO, 2011. 1, 5, 12
- [31] Sangwon Kim, Jaeyeal Nam, and Byoung Chul Ko. ViT-NeT: Interpretable vision transformers with neural tree decoder. In *Proceedings of the 39th International Conference on Machine Learning*, pages 11162–11172. PMLR, 2022. 2
- [32] Pang Wei Koh, Thao Nguyen, Yew Siang Tang, Stephen Mussmann, Emma Pierson, Been Kim, and Percy Liang. Concept bottleneck models. In *Proceedings of the 37th International Conference on Machine Learning*, pages 5338–5348. PMLR, 2020. 1, 2
- [33] Jonathan Krause, Michael Stark, Jia Deng, and Li Fei-Fei. 3d object representations for fine-grained categorization. In *Proceedings of the IEEE international conference on computer vision workshops*, pages 554–561, 2013. 1, 5, 12
- [34] Chunyuan Li, Cliff Wong, Sheng Zhang, Naoto Usuyama, Haotian Liu, Jianwei Yang, Tristan Naumann, Hoifung Poon, and Jianfeng Gao. Llava-med: Training a large language-and-vision assistant for biomedicine in one day. *arXiv preprint arXiv:2306.00890*, 2023. 1
- [35] Yuchao Li, Rongrong Ji, Shaohui Lin, Baochang Zhang, Chenqian Yan, Yongjian Wu, Feiyue Huang, and Ling Shao. Interpretable neural network decoupling. In *European Conference on Computer Vision*, 2019. 2
- [36] Haoyu Liang, Zhihao Ouyang, Yuyuan Zeng, Hang Su, Zihao He, Shu-Tao Xia, Jun Zhu, and Bo Zhang. Training interpretable convolutional neural networks by differentiating class-specific filters. In *European Conference on Computer Vision*, pages 622–638. Springer, 2020. 2
- [37] Haotian Liu, Chunyuan Li, Qingyang Wu, and Yong Jae Lee. Visual instruction tuning. In *Advances in Neural Information Processing Systems*, pages 34892–34916. Curran Associates, Inc., 2023. 1
- [38] Ilya Loshchilov and Frank Hutter. SGDR: Stochastic gradient descent with warm restarts. In *International Conference on Learning Representations*, 2017. 5
- [39] Ilya Loshchilov and Frank Hutter. Decoupled weight decay regularization. In *International Conference on Learning Representations*, 2019. 5
- [40] S. Maji, J. Kannala, E. Rahtu, M. Blaschko, and A. Vedaldi. Fine-grained visual classification of aircraft. Technical report, 2013. 1, 5, 12
- [41] Dmitrii Marin, Jen-Hao Rick Chang, Anurag Ranjan, Anish Prabhu, Mohammad Rastegari, and Oncel Tuzel. Token pooling in vision transformers for image classification. In *IEEE/CVF Winter Conference on Applications of Computer Vision, WACV 2023, Waikoloa, HI, USA, January 2-7, 2023*, pages 12–21. IEEE, 2023. 5
- [42] Meike Nauta, Annemarie Jutte, Jesper Provoost, and Christin Seifert. This looks like that, because... explaining prototypes for interpretable image recognition. In *Joint European Conference on Machine Learning and Knowledge Discovery in Databases*, pages 441–456. Springer, 2021. 2
- [43] Meike Nauta, Ron Van Bree, and Christin Seifert. Neural prototype trees for interpretable fine-grained image recognition. In *Proceedings of the IEEE/CVF Conference on Computer Vision and Pattern Recognition*, pages 14933–14943, 2021.
- [44] Meike Nauta, Jörg Schlötterer, Maurice van Keulen, and Christin Seifert. Pip-net: Patch-based intuitive prototypes for interpretable image classification. In *Proceedings of the IEEE/CVF Conference on Computer Vision and Pattern Recognition (CVPR)*, pages 2744–2753, 2023. 2
- [45] Tuomas Oikarinen, Subhro Das, Lam M. Nguyen, and Tsui-Wei Weng. Label-free concept bottleneck models. In *The Eleventh International Conference on Learning Representations*, 2023. 1, 2
- [46] Maxime Oquab, Timothée Darcet, Théo Moutakanni, Huy V. Vo, Marc Szafraniec, Vasil Khalidov, Pierre Fernandez, Daniel HAZIZA, Francisco Massa, Alaaeldin El-Nouby, Mido Assran, Nicolas Ballas, Wojciech Galuba, Russell Howes, Po-Yao Huang, Shang-Wen Li, Ishan Misra, Michael Rabbat, Vasu Sharma, Gabriel Synnaeve, Hu Xu, Herve Jegou, Julien Mairal, Patrick Labatut, Armand Joulin, and Piotr Bojanowski. DINOv2: Learning robust visual features without supervision. *Transactions on Machine Learning Research*, 2024. Featured Certification. 1
- [47] Zizheng Pan, Bohan Zhuang, Jing Liu, Haoyu He, and Jianfei Cai. Scalable vision transformers with hierarchical pooling. In *Proceedings of the IEEE/cvf international conference on computer vision*, pages 377–386, 2021. 5
- [48] O. M. Parkhi, A. Vedaldi, A. Zisserman, and C. V. Jawahar. Cats and dogs. In *IEEE Conference on Computer Vision and Pattern Recognition*, 2012. 1, 5, 12
- [49] DIPANJYOTI PAUL, Arpita Chowdhury, Xinqi Xiong, Feng-Ju Chang, David Edward Carlyn, Samuel Stevens, Kaiya L Provost, Anuj Karpatne, Bryan Carstens, Daniel Rubenstein, Charles Stewart, Tanya Berger-Wolf, Yu Su, and Wei-Lun Chao. A simple interpretable transformer for fine-grained image classification and analysis. In *The Twelfth International Conference on Learning Representations*, 2024. 2
- [50] Vitali Petsiuk, Abir Das, and Kate Saenko. Rise: Randomized input sampling for explanation of black-box models.

- In *Proceedings of the British Machine Vision Conference (BMVC)*, 2018. 2, 5
- [51] Maithra Raghu, Thomas Unterthiner, Simon Kornblith, Chiyuan Zhang, and Alexey Dosovitskiy. Do vision transformers see like convolutional neural networks? In *Advances in Neural Information Processing Systems*, 2021. 2
- [52] Mattia Rigotti, Christoph Mikovic, Ioana Giurgiu, Thomas Gschwind, and Paolo Scotton. Attention-based interpretability with concept transformers. In *International Conference on Learning Representations*, 2022. 2
- [53] Dawid Rymarczyk, Łukasz Struski, Michał Górszczak, Koryna Lewandowska, Jacek Tabor, and Bartosz Zieliński. Interpretable image classification with differentiable prototypes assignment. *Proceedings of the European Conference on Computer Vision (ECCV)*, 2022. 2
- [54] Ramprasaath R. Selvaraju, Michael Cogswell, Abhishek Das, Ramakrishna Vedantam, Devi Parikh, and Dhruv Batra. Grad-cam: Visual explanations from deep networks via gradient-based localization. In *2017 IEEE International Conference on Computer Vision (ICCV)*, pages 618–626, 2017. 2, 6, 12, 13
- [55] Sofia Serrano and Noah A. Smith. Is attention interpretable? In *Proceedings of the 57th Annual Meeting of the Association for Computational Linguistics*, pages 2931–2951, Florence, Italy, 2019. Association for Computational Linguistics. 1
- [56] Wen Shen, Zhihua Wei, Shikun Huang, Binbin Zhang, Jiaqi Fan, Ping Zhao, and Quanshi Zhang. Interpretable compositional convolutional neural networks. In *Proceedings of the International Joint Conference on Artificial Intelligence*, 2021. 2
- [57] Karen Simonyan and Andrew Zisserman. Very deep convolutional networks for large-scale image recognition. In *International Conference on Learning Representations*, 2015. 2
- [58] Karen Simonyan, Andrea Vedaldi, and Andrew Zisserman. Deep inside convolutional networks: Visualising image classification models and saliency maps. *arXiv preprint arXiv:1312.6034*, 2013. 1
- [59] Sarah Tan, Giles Hooker, Paul Koch, Albert Gordo, and Rich Caruana. Considerations when learning additive explanations for black-box models. *Mach. Learn.*, 112(9):3333–3359, 2023. 2
- [60] Hugo Touvron, Matthieu Cord, Matthijs Douze, Francisco Massa, Alexandre Sablayrolles, and Herve Jegou. Training data-efficient image transformers; distillation through attention. In *Proceedings of the 38th International Conference on Machine Learning*, pages 10347–10357. PMLR, 2021. 5, 12
- [61] Hugo Touvron, Matthieu Cord, and Hervé Jégou. DeiT iii: Revenge of the vit. In *European Conference on Computer Vision*, 2022. 5, 8
- [62] Yuki Ukai, Tsubasa Hirakawa, Takayoshi Yamashita, and Hironobu Fujiyoshi. This looks like it rather than that: ProtoKNN for similarity-based classifiers. In *The Eleventh International Conference on Learning Representations*, 2023. 2
- [63] Robert van der Klis, Stephan Alaniz, Massimiliano Mancini, Cassio F Dantas, Dino Ienco, Zeynep Akata, and Diego Marcos. Pdisconet: Semantically consistent part discovery for fine-grained recognition. In *Proceedings of the IEEE/CVF International Conference on Computer Vision*, pages 1866–1876, 2023. 2
- [64] Ashish Vaswani, Noam Shazeer, Niki Parmar, Jakob Uszkoreit, Llion Jones, Aidan N Gomez, Łukasz Kaiser, and Illia Polosukhin. Attention is all you need. *Advances in neural information processing systems*, 30, 2017. 2, 3
- [65] C. Wah, S. Branson, P. Welinder, P. Perona, and S. Belongie. The caltech-ucsd birds-200-2011 dataset. Technical Report CNS-TR-2011-001, California Institute of Technology, 2011. 1, 5, 12
- [66] Chong Wang, Yuyuan Liu, Yuanhong Chen, Fengbei Liu, Yu Tian, Davis J McCarthy, Helen Frazer, and Gustavo Carneiro. Learning support and trivial prototypes for interpretable image classification. In *Proceedings of the IEEE/CVF International Conference on Computer Vision*, pages 2062–2072, 2023. 1, 2
- [67] Jiaqi Wang, Huafeng Liu, Xinyue Wang, and Liping Jing. Interpretable image recognition by constructing transparent embedding space. In *Proceedings of the IEEE/CVF International Conference on Computer Vision (ICCV)*, pages 895–904, 2021. 2
- [68] Xue Wang, Zhibo Wang, Haiqin Weng, Hengchang Guo, Zhifei Zhang, Lu Jin, Tao Wei, and Kui Ren. Counterfactual-based saliency map: Towards visual contrastive explanations for neural networks. In *Proceedings of the IEEE/CVF International Conference on Computer Vision (ICCV)*, pages 2042–2051, 2023. 2
- [69] Mengqi Xue, Qihan Huang, Haofei Zhang, Jingwen Hu, Jie Song, Mingli Song, and Canghong Jin. Protopformer: Concentrating on prototypical parts in vision transformers for interpretable image recognition. In *Proceedings of the Thirty-Third International Joint Conference on Artificial Intelligence, IJCAI-24*, pages 1516–1524. International Joint Conferences on Artificial Intelligence Organization, 2024. Main Track. 2, 6
- [70] Hongxu Yin, Arash Vahdat, Jose Alvarez, Arun Mallya, Jan Kautz, and Pavlo Molchanov. A-ViT: Adaptive tokens for efficient vision transformer. In *Proceedings of the IEEE/CVF Conference on Computer Vision and Pattern Recognition*, 2022. 2, 5
- [71] Weihao Yu, Chenyang Si, Pan Zhou, Mi Luo, Yichen Zhou, Jiashi Feng, Shuicheng Yan, and Xinchao Wang. Metaformer baselines for vision. *IEEE Transactions on Pattern Analysis and Machine Intelligence*, 46(2):896–912, 2024. 8
- [72] Mehdi Zemni, Mickaël Chen, Éloi Zablocki, Hedi Ben-Younes, Patrick Pérez, and Matthieu Cord. Octet: Object-aware counterfactual explanations. In *IEEE Conference on Computer Vision and Pattern Recognition, CVPR*, 2023. 2
- [73] Quanshi Zhang, Ying Nian Wu, and Song-Chun Zhu. Interpretable convolutional neural networks. In *Proceedings of the IEEE conference on computer vision and pattern recognition*, pages 8827–8836, 2018. 2
- [74] Bolei Zhou, Aditya Khosla, Agata Lapedriza, Aude Oliva, and Antonio Torralba. Learning deep features for discriminative localization. In *Proceedings of the IEEE conference on computer vision and pattern recognition*, pages 2921–2929, 2016. 4, 5

# Supplementary Material

## A. Model architecture details

To compare our architecture as fairly as possible with standard methods (*i.e.*, DeiT [60]), we follow the same hyperparameter selection for both the base and small versions as their ViT equivalents. That is, HiT base (HiT-B) follows the same architecture as ViT-B. Similarly, HiT small (HiT-S) follows the same hyperparameters as ViT-S. The only differences are the pooling layers, the initial patch size, and that we have removed the last MLP block as it is not used. Tab. 4 shows the architecture hyperparameter choices compared to Visual Transformers.

Version	Layers	Feature dimension	Heads	Pooling layer location	Patch dimension	Parameter count
HiT-B	12	768	12	[4, 8]	8	81.8
ViT-B	12	768	12	-	16	86.9
HiT-S	12	384	6	[4, 8]	8	20.8
ViT-S	12	384	6	-	16	22.1

Table 4. HiT base and small hyperparameter configurations

## B. Datasets

As for the dataset, we evaluated HiT on six diverse image classification datasets: i) ImageNet [16]: A large-scale dataset with 1.2 million images and 1,000 classes, often used as a benchmark. ii) CUB-2011 [65]: A challenging dataset containing 200 bird classes with only 30 training samples per class on average. iii) Stanford Dogs [30]: A dataset with 120 dog classes and 10,000 training and test images. iv) Stanford Cars [33]: A dataset featuring 196 car classes with 8,100 training and validation examples. v) FGVC-Aircraft [40]: A dataset of 100 airplance classes with 10,000 images. vi) Oxford-IIIT Pets [48]: a 37 category dataset with roughly 200 images per class.

## C. Insertion-Deletion Curves

In Fig. 7, we present the curves from the post-hoc comparison experiment detailed in § 4.3 of the main document. HiT consistently outperforms both GradCAM [54] and Rollout Matrix [1] across all datasets. Interestingly, GradCAM achieves performance comparable to our method on all datasets except ImageNet [16]. We hypothesize that this correlation stems from GradCAM being computed on the final layer tokens, which our analysis shows are the most important (Fig. 5 in the manuscript), except for ImageNet.

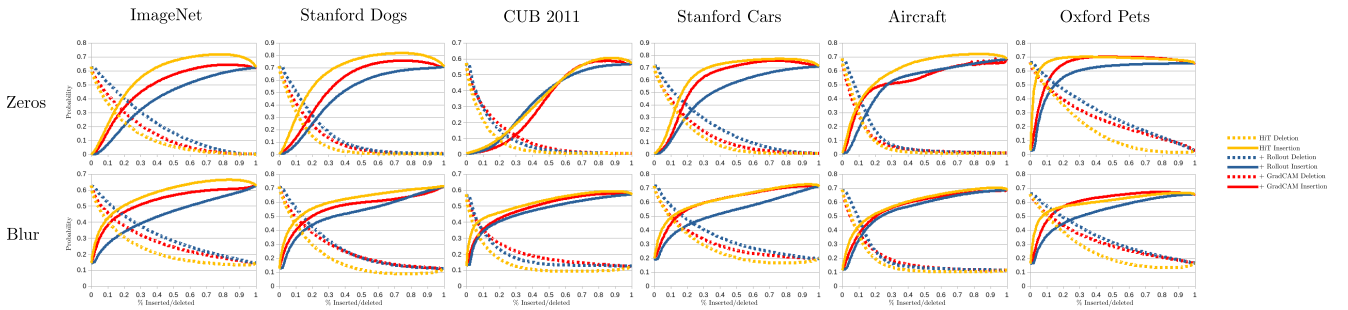


Figure 7. **Comparing HiT and alternative post-hoc methods.** This experiments reflects the interpretable advantages with respect to traditional post-hoc methods.

## D. Evaluating HiT without Pooling Layers

We conducted experiments similar to those in the main manuscript to analyze the positive and negative impact of removing pooling layers. As demonstrated in § 4.7 of the paper, pooling layers are essential for improving top-1 accuracy performance. However, their inclusion increases the size of the explanations. First, we explore this phenomenon quantitatively in sections D.1 and § D.2. Later, we will explore the qualitative differences in § D.3.



### D.1. Interpretability Trade-off

First, we explore the interpretability gains of HiT without pooling layers. We compare both HiT versions using the normalized insertion-deletion curves on all tested datasets, illustrated in Fig. 8. From a quantitative point of view, HiT without any pooling layer is even more interpretable than our proposed architecture. Interestingly, both curves behave similarly, showing a decrease in the insertion probability curve and an increase in the deletion probability curve during their final steps. This is due to the insertion (or deletion) of tokens that adversely affect the model’s prediction.

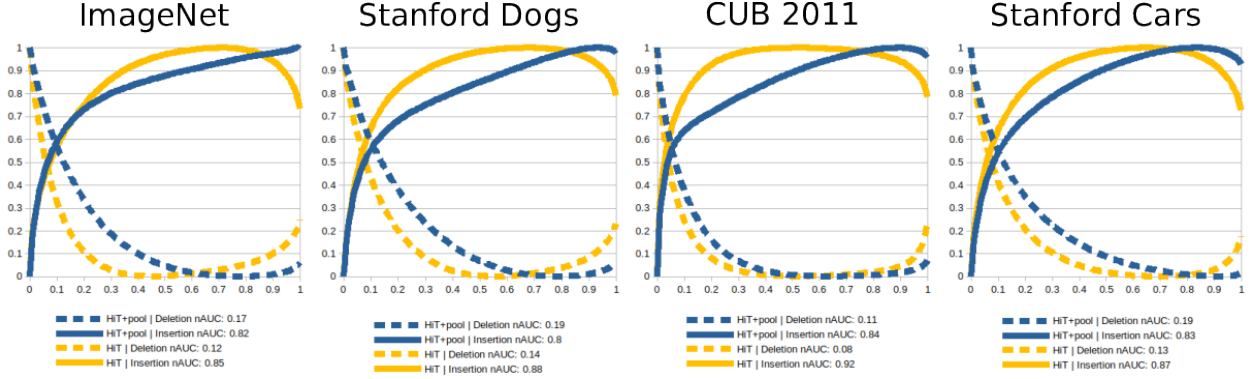


Figure 8. Caption

We also tested GradCAM [54] and the Rollout [1] Matrix directly on our pooling-free HiT architecture, with results shown in Table 5. The interpretability gap between post-hoc methods and HiT saliency maps is more pronounced compared to our standard HiT architecture.

Method	ImageNet		CUB 2011		Stanford Cars		Stanford Dogs	
	Ins-Z (↑)	Del-Z (↓)	Ins-Z (↑)	Del-Z (↓)	Ins-Z (↑)	Del-Z (↓)	Ins-Z (↑)	Del-Z (↓)
HiT	<b>0.65</b>	<b>0.08</b>	<b>0.56</b>	<b>0.04</b>	<b>0.72</b>	<b>0.05</b>	<b>0.64</b>	<b>0.07</b>
HiT + Rollout	0.39	0.21	0.43	0.09	0.49	0.12	0.47	0.19
HiT + GradCAM	0.36	0.15	0.40	0.09	0.34	0.11	0.40	0.15
Method	Ins-B (↑)		Ins-B (↑)		Ins-B (↑)		Ins-B (↑)	
	Del-B (↓)		Del-B (↓)		Del-B (↓)		Del-B (↓)	
HiT	<b>0.67</b>	<b>0.16</b>	<b>0.59</b>	<b>0.11</b>	<b>0.65</b>	<b>0.15</b>	<b>0.62</b>	<b>0.18</b>
HiT + Rollout	0.47	0.31	0.50	0.22	0.50	0.29	0.50	0.32
HiT + GradCAM	0.48	0.29	0.52	0.21	0.51	0.29	0.52	0.31

Table 5. **HiT and Explainability methods:** We quantitatively compare HiT maps and those created by GradCAM and the modified rollout matrix (mean attention). The assessment shows that HiT maps are in fact more faithful to those generated by GradCAM and the rollout matrix. Higher insertion is better, while lower deletion is better. Ins and Del refers to the Insertion and Deletion metrics, respectively. Z is the zero-corrupted image, while B is the blurred corruption strategy.

Finally, in Tab. 6, we show the performance on the tested datasets. Without any surprise, the loss in performance is major, making it a less appealing option in contrast to our original architecture when computation power is needed.

### D.2. Layer-wise Contributions

Next, we investigate the ability of the pooling-free HiT to analyze layer-wise contributions. Fig. 9a illustrates the layer contribution per dataset, while Fig. 9b plots the ablation results on ImageNet [16]. Similar to HiT with layer pooling, the most significant contributions come from the final layers. However, unlike the HiT version with pooling layers, all trained models appear to weight their final predictions equally across the last three layers.

### D.3. Qualitative Comparison

Finally, we qualitatively show the difference between the pool-free HiT and our original version saliency maps in Fig. 10 in ImageNet [16]. As expected, removing the pooling layers produces finer saliency maps.

Model	Pooling?	ImageNet	CUB	Dogs	Cars
HiT-S	$\chi$	67.3	76.1	77.1	83.9
	$\checkmark$	71.4	76.1	80.3	85.2
HiT-B	$\chi$	71.5	76.3	80.2	84.7
	$\checkmark$	75.0	79.0	86.8	86.2

Table 6. **Top1 Accuracy.** Including pooling layers provides a clear advantage in terms of raw performance. However, this performance gain comes at the cost of reduced interpretability.

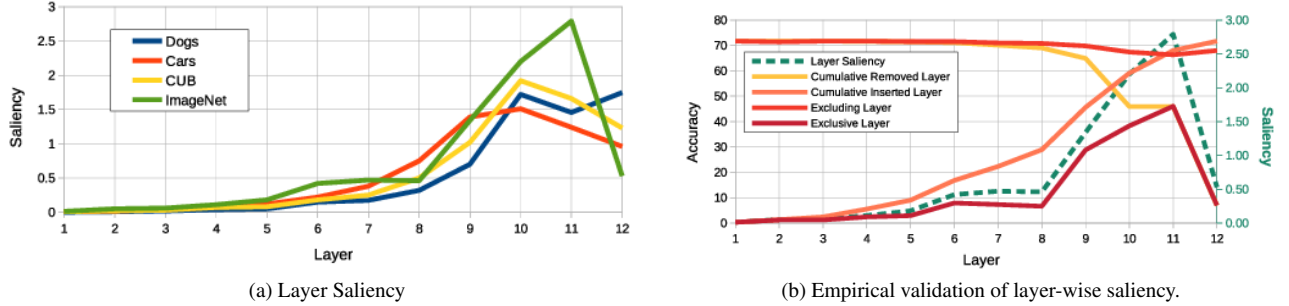


Figure 9. As in the main manuscript, we assess our pooling-free HiT layer contribution. Effectively, HiT can discover the contributions for each layer.

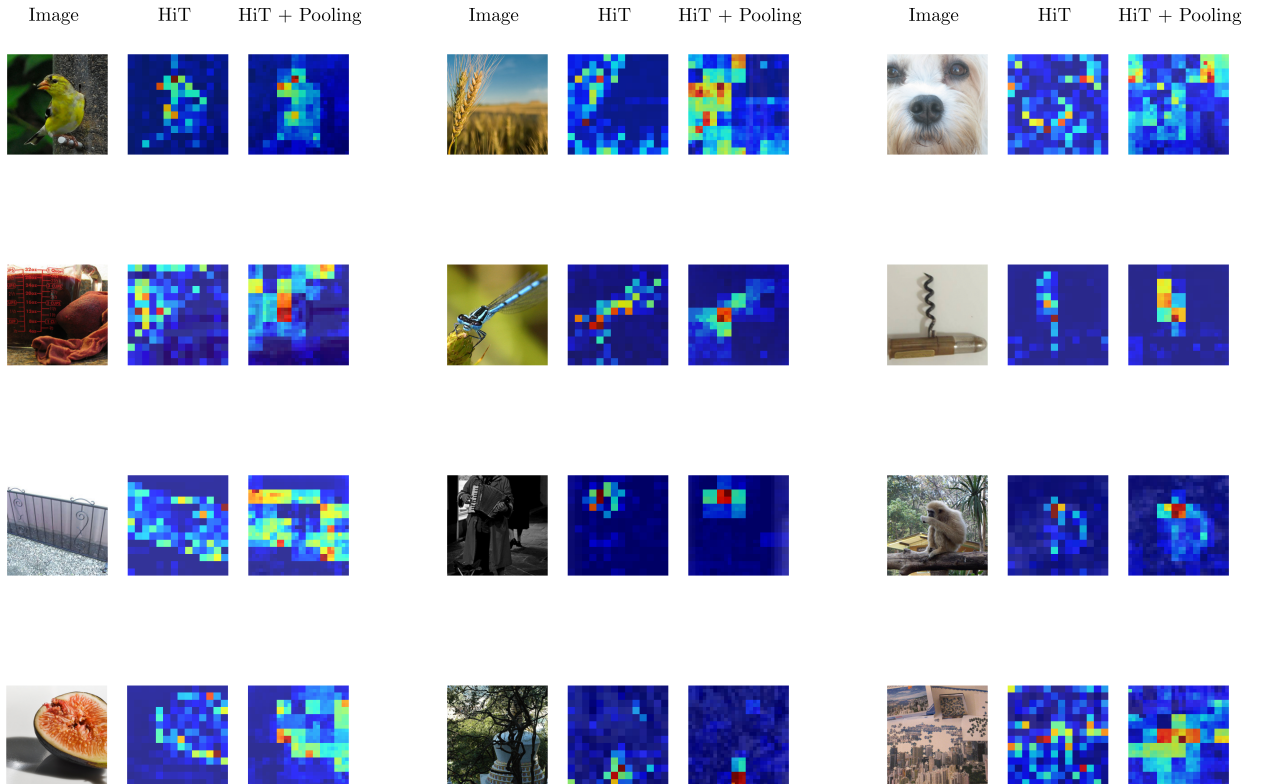


Figure 10. **Qualitative Examples:** we visually show the difference between HiT saliency maps with and without pooling layers on some correctly classified images from the ImageNet dataset.